Detection and quantitation of cellulose II by Raman spectroscopy

Umesh P. Agarwal (umesh.p.agarwal@usda.gov)
Fiber and Chemical Sciences Research, USDA FS, Forest Products Laboratory

Sally A. Ralph
Fiber and Chemical Sciences Research, USDA FS, Forest Products Laboratory

Carlos Baez
Fiber and Chemical Sciences Research, USDA FS, Forest Products Laboratory

Richard S. Reiner
Fiber and Chemical Sciences Research, USDA FS, Forest Products Laboratory

Research Article

Keywords: Cellulose II, detection, quantitation, mixture of cellulose I and II, Raman, XRD

Posted Date: June 28th, 2021

DOI: https://doi.org/10.21203/rs.3.rs-661415/v1

Detection and quantitation of cellulose II by Raman spectroscopy

Umesh P. Agarwal[a],[*] , *Sally A. Ralph*[a], *Carlos Baez*[a], *Richard S. Reiner*[a]

[a]Fiber and Chemical Sciences Research, USDA FS, Forest Products Laboratory, 1 Gifford Pinchot Drive Madison, WI 53726-2398

[*]To whom correspondence should be addressed. Email: umesh.p.agarwal@usda.gov

ABSTRACT

In cellulose materials, the cellulose II polymorph is often present either exclusively or in conjunction with cellulose I, the natural cellulose. Moreover, in regenerated and mercerized fibers (e,g., viscose and lyocell), natural cellulose adopts to the crystal structure cellulose II Therefore, its detection and quantitation are important for a complete assessment of such materials investigations. In the Raman spectra of such materials, a band at 577 cm^{-1} is typically observed indicating the presence of this polymorph. In the present study, to quantify the content of cellulose II, a calibration method was developed based on the intensity of the 577 cm^{-1} peak relative to the 1096 cm^{-1} band of cellulose. For this purpose, in addition to pure cellulose I and cellulose II samples (respectively, Avicel PH-101 and mercerized Avicel PH-101; hence referred to as Avicel I and Avicel II), a set of five samples were produced by mixing them in known quantities of Avicel I and Avicel II. The crystalline cellulose II contents of the samples were calculated based on the X-ray crystallinity of mercerized Avicel I. These seven samples were included in the calibration set and their Raman spectra were obtained. Subsequently, Raman intensity ratios I_{577}/I_{1096} were calculated by taking ratios of peak intensities at 577 and 1096 cm^{-1}. These ratios were plotted against the % of crystalline cellulose II present in the calibration set samples and the two were

found to be linearly correlated (R^2 = 0.9944). The set-samples were also analyzed using XRD which were then compared with the Raman method developed here. Compared to XRD, the Raman method was found to be more sensitive at detecting and quantifying cellulose II. Additionally, several cellulose II containing materials were analyzed by the new Raman method.

INTRODUCTION

Raman spectroscopy is being increasingly used to investigate celluloses and cellulose based materials (Agarwal, 2019; Agarwal et al., 2021a; Agarwal et al., 2021b; Gierlinger et al., 2018; Kanbayashi et al., 2021; Kesari et al., 2020; Morgan et al., 2019). One of the areas of interest where development is urgently needed is the area of cellulose supramolecular structure characterization which is of importance in many areas of bioeconomy R & D, e.g., biofuels (Callegari et al., 2020) and nanocellulose based materials (Foster et al., 2018). The characterization is needed to understand how different process conditions affect the supramolecular structure of cellulose. Towards that objective, Raman spectroscopy has already made several significant contributions. For instance, methods based on three different Raman peaks – 1481, 380, and 93 cm^{-1}, have been developed to estimate cellulose crystallinity (respectively, Schenzel et al., 2005; Agarwal et al., 2010; Agarwal et al., 2018). Similarly, Raman methods to measure other characteristics of the structure, such as accessibility to water (Agarwal et al., 2016; Foster et al., 2018), degree of lateral order (DOLO) (Agarwal et al., 2016), exocyclic C6 CH_2OH conformation (Agarwal et al., 2018; Agarwal et al., 2021b), and chain conformational disorder (CCONDIS) (Agarwal et al., 2021b) have been established so that cellulose materials can be better characterized and understood. Considering that there is a lack of existing methods to define the supramolecular structure of cellulose, the contribution of Raman spectroscopy is a welcome development.

Cellulose can exist in various crystalline forms and therefore, is a polymorphic material. There are four distinct known forms - cellulose I, cellulose II, cellulose III, and cellulose IV, although the existence of cellulose IV is still debated (Wada et al., 2004; Wada et al., 2006). For instance, cellulose IV_I and cellulose IV_{II} are, respectively, considered disordered forms of cellulose I and cellulose II, or in the case of cellulose IV_{II}, as a mixture of cellulose I and cellulose II (Wada et al., 2004). Moreover, for cellulose I, two distinct crystalline forms have been proposed – Iα and Iβ (Atalla & VanderHart, 1984). Cellulose II (also referred to as regenerated and mercerized cellulose) is the other most often used polymorph. The regenerated form is produced by dissolution - e.g., from ionic liquids (Sixta et al., 2015) and the mercerized form is produced from NaOH-swelled cellulose (Porro et al., 2007). The latter is used in viscose rayon manufacture in the textile and fiber industries (Kumar and Christopher, 2017). Cellulose II is also formed during many laboratory and industrial processes; e.g., cellulose nanocrystal production during sulfuric acid hydrolysis of wood-pulps (Xing et al., 2018), in the manufacturing of dissolving pulps (Chen et al., 2016), and in the production of regenerated cellulose for use in textile fibers (Sixta et al., 2015). Mercerization to produce cellulose II is used in the textile industry to help natural fibers gain shine, dyeability, and strength. Moreover, the same process is used as an activation step for many industrial products such as cellulose derivatives, regenerated fibers, and cellulose-based sponges. From a structural point of view, cellulose I and cellulose II polymorphs differ not only in that their H-bonds are different, but also conformations of the chains and the local exocyclic C_6 hydroxyl groups are different (Atalla, 1976, 1983, 1989). Additionally, contrary to cellulose I where the chains have parallel orientation, in cellulose II, the chains are stacked with opposite polarity, also called an antiparallel structure (Langan et al., 2001).

Because the properties of the cellulose II polymorph are different from those of cellulose I (Sixta et al., 2015), the characterization of the former is essential. For that purpose, some of the often-used methods consist of X-ray, NMR and Raman spectroscopy (Nam et al., 2016; Nishiyama et al., 2000; NMR : Atalla et al., 1980; Haslinger et al., 2019; Atalla, 1976; Schenzel and Fischer 2001). Amongst these techniques, XRD has been used the most to detect and obtain information on cellulose II (Zugenmaier, 2010). However, in materials where both cellulose I and cellulose II polymorphs are simultaneously present, typically, in most methods, such analyses are based on the separation of cellulose II contributions from the contributions of cellulose I. Therefore, the analyses remain somewhat subjective, especially when there is significant overlap between the contributions.

Traditional Raman spectroscopy has been applied for a long time in the analysis of cellulose materials, but due to sample-fluorescence contributions to the spectra, it was not until FT-Raman spectroscopy became available that high signal-to-noise spectra could be obtained (Agarwal 1997, 1999; Schenzel and Fischer, 2001). The first FT-Raman study of the transformation of cellulose I to cellulose II polymorph was reported in 2001 (Schenzel and Fischer 2001). Subsequently, in 2009, a multivariate calibration model based on FT Raman spectroscopy was developed to quantify cellulose I to cellulose II polymorphic transformation (Schenzel et al., 2009). However, this chemometric method is somewhat involved and not very user-friendly. Our intent was to develop a simple and more convenient Raman method. Previously, Agarwal (Agarwal, 2014) had compared the FT-Raman spectra of the three cellulose polymorphs (cellulose I, cellulose II, and cellulose III) and noted spectral differences between them in the conformation sensitive region (< 1500 cm^{-1}). Based on that information, cellulose I and cellulose II can be

distinguished easily. In particular, the existence of a band at 577 cm^{-1} in the spectrum of cellulose II can be seen which is not detected in the spectra of cellulose I and amorphous cellulose.

In many materials amorphous cellulose is also present along with the cellulose I and cellulose II polymorphs It is critical that spectral features that are unique to cellulose II which do not overlap with the other Raman peaks in the spectrum of amorphous cellulose be used in its quantitation. Therefore, in this study, detection and quantitation of cellulose II was carried out using this 577 cm^{-1} band.

MATERIALS AND METHODS

Chemicals and materials. Avicel PH-101 (cellulose I) and Avicel-C (cellulose II) were obtained from American Viscose Division and Chemical Division of FMC Corporation, Newark, Delaware. Amorphous cellulose was generated by grinding, for 120 min, Avicel PH-101 in a vibratory mill using steel balls (Agarwal et al., 2010) and the milling was conducted in a cold room (5 °C). All other chemicals and reagents, unless stated otherwise, were purchased from Sigma-Aldrich (St. Louis, MO). Softwood bleached kraft pulp was from NewPage Corporation, Miamisburg, Ohio. Rayon-grade dissolving wood pulp used in the production of cellulose nanocrystals (CNCs) was obtained from Rayonier Mill in Jesup, GA.

Cellulose II preparation. Cellulose II was produced by mercerization following the method of Hirota (Hirota et al., 2010) with slight modification. The method consisted of soaking the Avicel sample (10 g) in 20% NaOH solution for 24 hrs while stirring. The material developed a pale-yellow color. After 24 hours, the mixture was filtered through a sintered glass funnel. The NaOH

solution filtered very slowly. A dilute HCl solution of ethanol/water (40%) was used for one rinse to bring the pH under 7. This was followed by additional washing with ethanol/water. The material was vacuum-dried at 50 °C before further use.

Calibration set samples. Cellulose mixtures with cellulose II compositions in the range of 5 – 80% were produced using different mass fractions of Avicel PH-101 (cellulose I called Avicel I) and mercerized Avicel-PH-101 (cellulose II called Avicel II). In each case, a total mixture mass of 500 mg was produced (Table 1). This group of five samples (mixtures 1–5, Table 1) along with the Avicel I and Avicel II samples were classified as a calibration set for the cellulose II quantitation analysis. The crystallinity of the Avicel II sample was determined using XRD and the method of Nam (Nam et al., 2016) to be 78.8%. The X-ray peaks at 21.7° and 16° 2θ, respectively, were used for the crystalline and amorphous contributions.

Table 1: Compositions of calibration set samples

Sample	Mass ratio, mg Avicel I:Avicel II	Avicel II, %	Calculated crystalline cellulose II, %*	Model-based cellulose II, %	% Error**
Avicel I	500:0	0	0	3.3	NA***
Mixture 1	475:25	5	3.94	5.2	32.0
Mixture 2	450:50	10	7.88	5.6	28.9
Mixture 3	400:100	20	15.8	14.5	8.2
Mixture 4	300:200	40	31.5	27.7	12.1
Mixture 5	100:400	80	63.0	62.7	0.5
Avicel II	0:500	100	78.8	78.6	0.3

*Based on XRD crystallinity of Avicel II (78.8%); **%Error calculated from the difference between model-based cellulose II and theoretical crystalline cellulose II amounts; ***NA, not applicable

Cellulose nanocrystals preparation. A procedure published earlier (Reiner and Rudie, 2013) was used to produce CNCs. Briefly, dissolving pulp was treated with sulfuric acid (64 wt%) and heated

to 45 °C for 90 minutes. The reaction was then quenched by transferring the suspension into a reactor containing a large amount of water. The suspension was further diluted. The CNC suspension is then neutralized by the slow addition of 5 – 8 wt% NaOH. The CNC solution is allowed to settle and is decanted. Upon further dilution, as the sodium sulfate concentration drops to about 1 wt%, the CNC particles begin to disperse in the solution. This aqueous suspension is then transferred to the ultrafiltration system for further purification. The CNCs are circulated through a tubular ultrafiltration system (Membrane Specialists, A19 modules), where the dilute salt/sugar solution passes through the membrane while CNCs are retained. Reverse osmosis (RO) water is added as needed to maintain the CNC concentrate at 1 wt%. Dialysis filtration is continued until the residual salt concentration is reduced to about 8 μM, (measured as 40–50 μS/cm2). This step requires about 24 hours of dilution and filtration The colloidal CNC suspension is filtered using a 20 μm polypropylene, cartridge-style filter to remove dirt and concentrated to at least 5 wt% solids using the tubular ultrafiltration system. The overall yield is about 50 wt%.

Alkali treatment of pulp. In a Berghof reactor (Berghof Inc., Eningen, Germany), air dried softwood bleached kraft pulp (SWBKP) (300 mg) was added to 40 mL of 5 or 10% NaOH solution and treated at 170 °C for 90 min. Post-treatment, the reactor was cooled by placing the vessel in a cold-water bath. The pulps were filtered through sintered glass funnels and were copiously washed with RO water until the filtered water was of neutral pH. Subsequently, the pulps were air dried at 25 °C.

Analysis by Raman spectroscopy. The calibration set and other samples were analyzed with a Bruker MultiRam FT-Raman spectrometer (Bruker Instruments Inc., Billerica, Massachusetts). This Raman system is equipped with a 1,064-nm 1,000-mW continuous wave (CW) diode-pumped Nd:YAG laser. Approximately 100 mg of each sample was pressed into a pellet with the help of a

hydraulic press. To make a pellet, a compressive pressure of 276 x 10^6 dyn/cm^2 was applied. Spectra were obtained in triplicate. The laser power used for sample excitation was 600 mW, and 1,024 scans were accumulated. In all cases, Bruker OPUS 7.2 software was used to process the spectral data, these operations involved normalization, selection of a spectral region, background correction, and band integration. Background correction was performed using a 64 points OPUS "rubberband option". For plotting purposes, the spectra were converted to ASCII format and exported to Excel.

Using FT-Raman spectroscopy, a cellulose II quantitation method was developed based upon the ratios of peak intensities at 577 (cellulose II band) and 1096 cm^{-1} (band due to both cellulose I and cellulose II). The ratios were plotted against the calculated % cellulose II, shown in Table 1. For calculating the peak heights, the following procedures were used. For both the bands, 577 and 1096 cm^{-1}, horizontal baselines were drawn from, respectively, 590 and 944 cm^{-1} and the peak heights were measured. For the ratios I_{577}/I_{1096}, the standard deviations (SDs) were < 2.5% except for mixtures 2 and 3 where the SDs were 6 and 10%, respectively. .

Analysis by X-ray. Wide-angle X-ray diffraction (XRD) profiles were recorded at the Materials Research Science and Engineering Center, University of Wisconsin, Madison using a Bruker (Billerica, MA) D8 Discover diffractometer in reflection mode with 0.5 mm beam aperture and equipped with monochromatic CuKα (k = 1.5418 Å) point source and a VÅ NTEC-500

detector. The X-ray diffractometer beam aperture of 0.5 mm was used. In all cases, diffractograms were obtained on the same samples (in pellet form) that were previously analyzed by FT-Raman spectroscopy.

. The crystallinity of the cellulose II sample (Avicel II) was determined using the XRD method of Nam (Nam et al., 2016). The X-ray peaks at 21.7° and 16° 2θ representing, respectively, crystalline and amorphous contributions were used. For each of the calibration set samples (Table 1), using the Avicel II crystallinity data (78.8%, Table 1), the following Eq. was used to calculate the "calculated crystalline cellulose II" content. This value represented the actual amount of crystalline cellulose II present in the samples.

$$\%\ Calculated\ crystalline\ cellulose\ II\ =\ Crystallinity\ of\ Avicel\ II * (\%\ Avicel\ II) \quad (1)$$

Where "% Avicel II" is the mass of Avicel II present in each of the samples (Table 1).

RESULTS AND DISCUSSION

The compositions of various calibration set samples are shown in Table 1. In total, there are seven samples including two samples of the "pure" cellulose polymorphs (Avicel I and Avicel II), because the two polymorphs are not 100% crystalline, they do contain some amorphous/disordered cellulose. For Avicel I and Avicel II, the Segal crystallinities (Segal et al., 1959) were, respectively, 87.5 (Agarwal et al., 2016) and 78.8% (Table 1).

The Raman spectra, in the region 250 - 1550 cm^{-1}, of Avicel I, Avicel II, and amorphous Avicel are shown in Fig. 1 and the spectral band positions are compared in Table 2. The assignments of the bands to various internal coordinates are from literature (Wiley and Atalla, 1987; Edwards et al., 1997) but it should be noted that most of the cellulose vibrational modes are

highly coupled (Wiley and Atalla, 1987) and therefore, the assignments are approximate. From the spectra and the Table, it can be noted that the mercerization treatment caused formation of cellulose II which leads to the appearance of several new spectral features (e.g., peaks at 353, 577, and 1463 cm^{-1}) and significant changes in the intensities or profiles of many Raman bands (e.g., 900 and 1263 cm^{-1}) all implying that molecular conformation in cellulose II is different from that of cellulose I (Atalla 1976, 1983, 1989; Schenzel and Fischer 2001; Wiley and Atalla, 1987). Of the many bands characterizing this polymorph (Table 2), the 577 cm^{-1} band is unique because it does not occur in the Raman spectra of either cellulose I or amorphous cellulose (Table 2, Fig. 1). Therefore, this cellulose II Raman band was selected to develop the calibration method reported here.

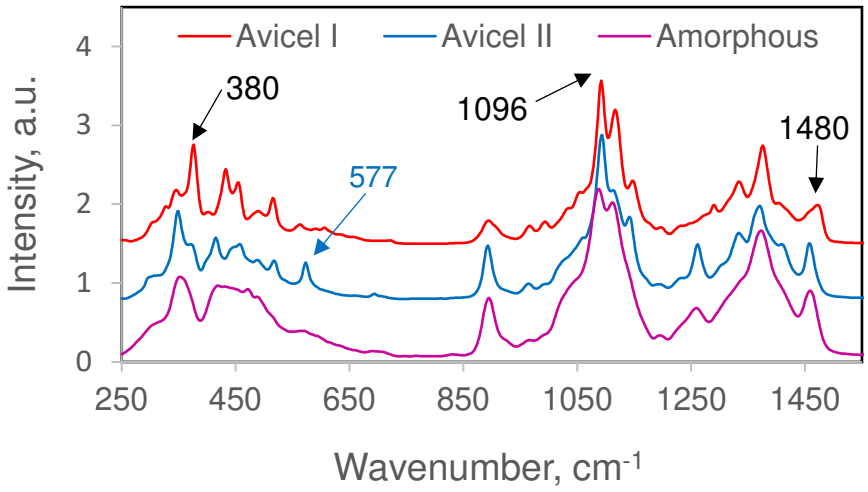

Figure 1: Raman spectra, in the region 250 – 1550 cm^{-1}, of Avicel I, Avicel II, and amorphous cellulose. Except for the 577 cm^{-1} band, all other annotated bands are in the spectrum of Avicel I.

Table 2: Raman frequencies (250 – 1550 cm^{-1}) of cellulose I, cellulose II, and amorphous cellulose

Avicel I	Avicel II	Avicel Amorphous	Assignments* (Wiley and Atalla, 1987; Edwards et al., 1997)
—**	308(sh)	308(sh)	τ(COH)
331(sh)***	—	—	Heavy atom bending; ring twisting
348(w)	353(m)	356(m)	some heavy atom stretching;
381(m)	376(sh)	—	some heavy atom stretching; δ(CCC) ring
406 (vw)	—	—	—
—	419(m)	423(w)	—
437(m)	450(sh)	436(sh)	some heavy atom stretching; ν(CCO) ring
459(m)	461(m)	—	some heavy atom stretching; ν(CCO) ring
—	—	475(w)	some heavy atom stretching; ν(CCO) ring
492(w)	492(w)	492(sh)	some heavy atom stretching; ν(CCO) glycosidic
520(m)	522(m)	568(sh)	some heavy atom stretching; ν(CCO) ring glycosidic
567(w)	—	—	some heavy atom stretching
—	577(m)	—	some heavy atom stretching
595(vw)	—	—	δ(CCH) twisting
610(vw)	—	—	δ(CCH) twisting
725 (vw)	—	—	—
898(m)	—	—	ν(COC) in plane symmetric
912(sh)	—	—	HCC and HCO bending at C-6; ν(COC) in plane sym.
971(w)	969(w)	970(vw)	heavy atom (CC and CO); ρ(CH2)
997(w)	1000(sh)	—	Stretching, C-C and C-O; ρ(CH2)
—	1028(sh)	—	Stretching, C-C and C-O; ν(CO)
1037(sh)	—	—	Stretching, C-C and C-O; ν(CO) primary OH
—	—	1048(sh)	Stretching, C-C and C-O; ν(CO)
1059(sh)	1061(sh)	—	Stretching, C-C and C-O; ν(CO) secondary OH
1096(s),	1097(s)	1092(s)	Stretching, C-C and C-O; ν(COC) glycosidic asym.
1121(s)	1117(sh)	1116(s)	Stretching, C-C and C-O; ν(COC) in plane sym.
1152(m)	1146(m)	—	heavy atom stretching plus, HCC and HCO bending; ν(CC) ring breathing asym.
1201(vw)	1197(vw)	1199(vw)	δ(COH); δ(CCH)
1237(vw)	1237(vw)	—	δ(COH) out of plane
—	1265(m)	1263(m)	HCC and HCO bending; δ(CH2); δ(CH2) twisting
1294(m)	—	—	HCC and HCO bending; δ(CH2) twisting
1339(m)	1338(m)	—	HCC, HCO, and HOC bending; δ(CH2)
1380(m)	1374(m)	1377(s)	HCC, HCO, and HOC bending; δ(CH2)
1409(sh)	1413(sh)	—	HCC, HCO, and HOC bending; δ(CH2)
1463(sh)	1462(m)	1463(m)	HCH and HOC bending; δ(CH2) scissors
1476(m)	—	—	HCH and HOC bending; δ(CH2) scissors

* ν = stretching, δ = in plane scissoring, ρ = in plane rocking, τ = out of plane twisting
**"—" No band present near the wavenumber position(s) of the band(s) in other columns.

***Relative band intensities in a spectrum are indicated by s = strong, m = medium, w = weak, vw = very weak, and sh = shoulder.

209

210

211 Raman spectra of the two polymorphs and the five mixtures (Table 1) are shown in Figs.
212 2 and 3. The plotted spectra were normalized on the cellulose band at 1096 cm^{-1}. In Fig. 2,
213 spectra are shown in the spectral region 250 – 1550 cm^{-1}, whereas in Fig. 3, the expanded spectra
214 in the 577 cm^{-1} region are shown so that this band can be better visualized. In the spectra of the
215 calibration set samples, band profiles and intensities changed in the entire 250 – 1550 cm^{-1}
216 region. For instance, band intensities increased at 353, 577, 900, 1265, and 1462 cm^{-1}, these
217 being spectral positions where cellulose II contributes in Raman spectroscopy (Agarwal, 2014;
218 Schenzel and Fisher, 2001). As Avicel II content increased in the samples so did the band
219 intensity at 577 cm^{-1} (Figs. 2 and 3). The Raman intensity ratios I_{577}/I_{1096} were calculated and the
220 ratios were plotted against the % crystalline cellulose II present in the seven calibration set
221 samples (Figure 4). The ratios were found to be linearly correlated with the amounts of cellulose
222 II (Fig. 2, $R^2 = 0.9944$).

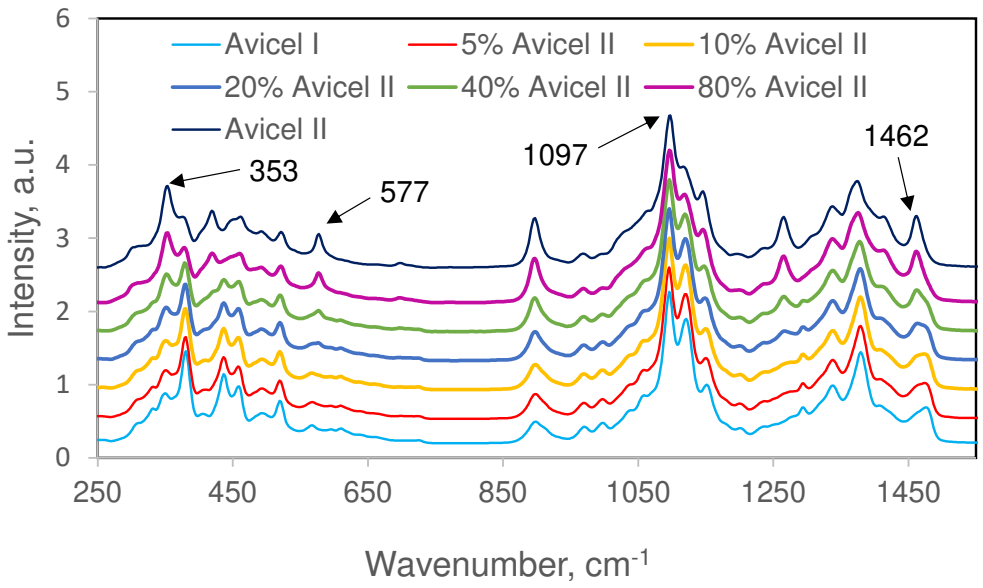

223

224 Figure 2: 250 – 1550 cm^{-1} region Raman spectra of Avicel I, Avicel II, and mixtures of Avicel I
225 and Avicel II. The annotated band positions are of Avicel II.

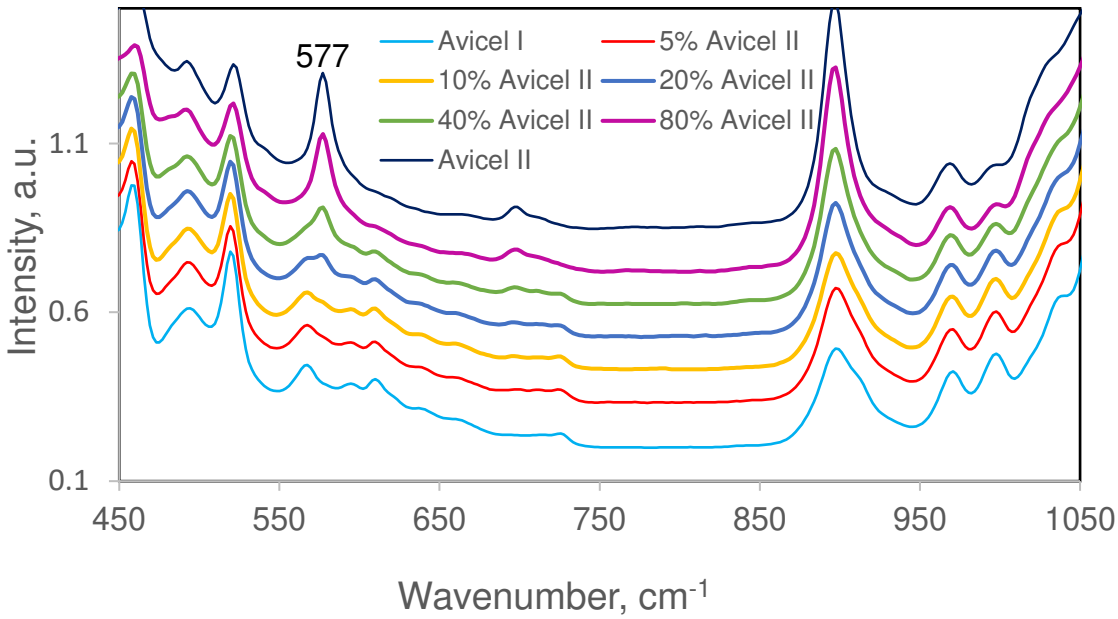

226

227 Figure 3: Expanded Raman spectra showing contributions at 577 cm^{-1} of the seven calibration
228 set samples.

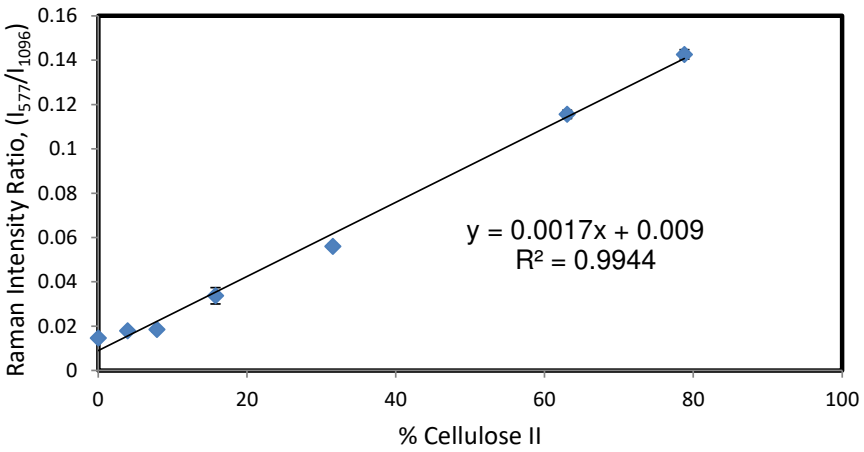

Figure 4: Correlation between Raman intensity ratio I_{577}/I_{1096} and crystalline cellulose II content of the calibration set samples. In most cases, the SD was < 2.5%.

Therefore, from the Raman spectrum of a sample that contains cellulose II polymorph, the following Eq. can be used to estimate the amount of crystalline cellulose II.

$$\%\ Cellulose\ II\ =\ [(I_{577}/I_{1096})\ -\ 0.009]/0.0017 \qquad (2)$$

The model-calculated values of all the samples are shown in Table 1 and it can be noted that compared to higher cellulose II concentrations, at low concentrations the error increases (Table 1). This larger error is because not only the 577 cm^{-1} peak of cellulose II becomes weaker but also because there is an increased cellulose I spectral contribution present at 577 cm^{-1} from the decaying wing of the nearby cellulose I band at 567 cm^{-1} (Fig. 3, Table 2). The effect of this overlap is evident in Table 1 where, in the absence of cellulose II, pure cellulose I sample still gives a value of 3.3% cellulose II. As the content of cellulose I relative to cellulose II declines, the 577 cm^{-1} contribution due to the former also declines and consequently, a better match between the theoretical and the model data is obtained (Table 1).

Comparison with XRD

To determine the usefulness of the Raman cellulose II quantitation method, it was compared with the XRD. In the latter technique, cellulose II is detected using the diffraction peaks present at 12.3, 20.5, and 22.0° 2θ (Fig. 5). Fig. 5 also shows the diffraction peaks of Avicel I and from the two XRDs, it can be noted that the cellulose II and cellulose I peaks, respectively, at 22 and 22.8° 2θ overlap significantly. Moreover, the lower-2θ side decaying wing of the 22.8° cellulose I peak has some contribution in the region 20.5° 2θ where the maximum of cellulose II peak is located (Fig. 5).

Shown in Fig. 6 are the XRDs of the calibration set samples and it can be seen that although at high Avicel II concentrations its diffraction peaks can be seen, none of the cellulose II peaks are detectable below 20 wt% concentration (Fig. 6). Compared to the 12.3° 2θ contribution, the peak at 20.5° is more easily detected although at 20 wt% composition the latter is still detected only as a weak shoulder. This is because the higher-2θ diffraction peak is more intense compared to the peak at 12.3° (Fig. 5). Nevertheless, as the concentration of Avicel II declines and the concentration of Avicel I increases, the contribution of the latter at 20.5° 2θ increases and the contribution of the former becomes unnoticeable. This observation is supported by a study that reported results of X-ray analysis of the blends of control and mercerized cotton fibers with various compositions (Nam et al., 2016). Likewise, in that study, at 20 wt% concentration of mercerized cotton fibers (cellulose II), the two diffraction peaks of the cellulose II polymorph could hardly be detected. When this detection limitation of 20 wt% in XRD is compared with Raman spectroscopy, the latter was found to be more sensitive because even at 5 wt% Avicel II composition, the spectral contribution at 577 cm^{-1} could be detected and measured (Figs. 3 and 4).

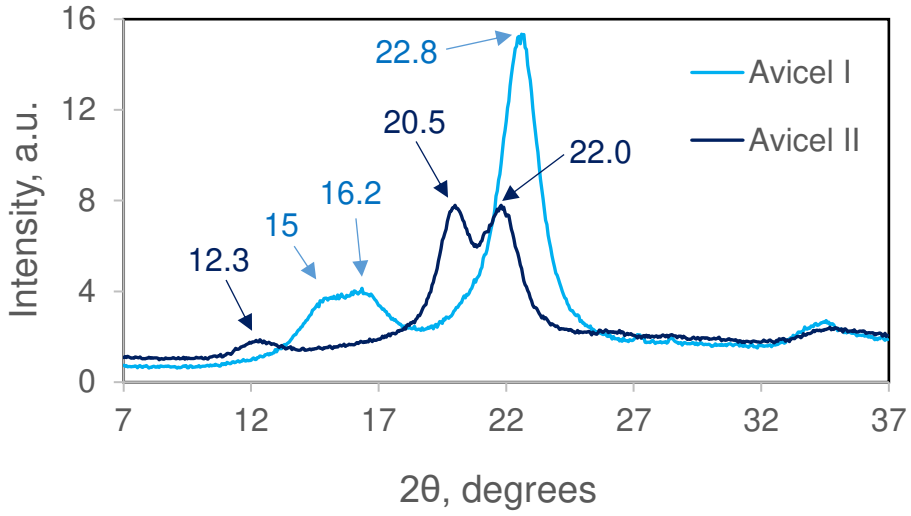

268

269 Figure 5: XRDs of Avicel I and Avicel II samples.

270

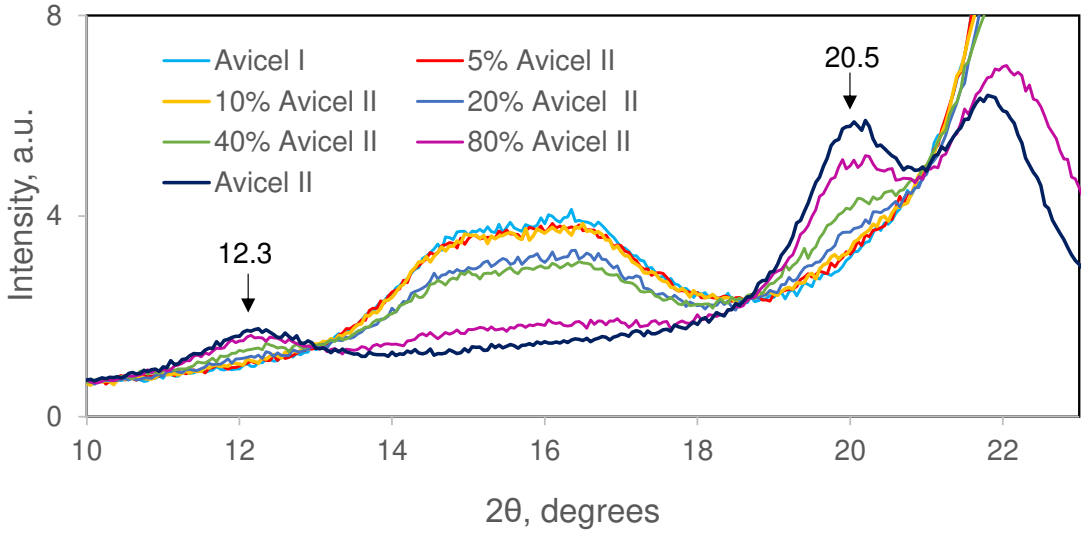

271

272 Fig. 6: XRDs of the calibration set samples

273

Applications

Next, we will examine some situations where in the materials either only cellulose II is present or both cellulose I and cellulose II coexist. Additionally, amorphous cellulose is usually present in various materials unless special treatment has been carried out (e.g., acid hydrolysis). The first of the four materials discussed here (Table 2), is bleached softwood kraft pulp (SWBKP) which, to remove hemicelluloses, was treated at 170 °C, at two NaOH concentrations – 5% and 10%. While the lower alkali concentration did not impact the crystal lattice of the pulp fibers, treatment by the 10% alkali partially converted the pulp fibers to cellulose II type (Fig. 7). In Fig. 7, Raman spectra, in the region 250 – 1550 cm^{-1}, of control and alkali-treated pulps are shown, and it can be noted that only the pulp treated with 10% alkali showed bands at 353 and 577 cm^{-1} implying that cellulose II had formed. The amount present was calculated using Eq. 2 and was found to be 35.5% as reported in Table 2. Moreover, the presence of a 380 cm^{-1} peak in the spectrum of 10% NaOH treated pulp (Fig. 7) indicated that a significant amount of cellulose I survived the transformation to cellulose II.

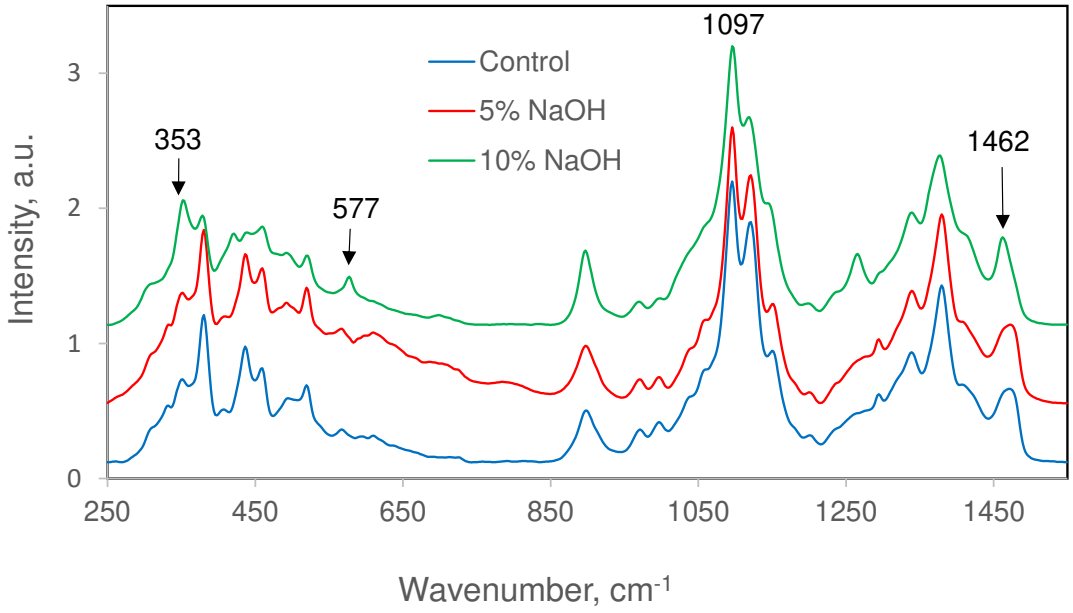

288

289 Fig. 7: Raman spectra of untreated (control) and alkali-treated (5% and 10% NaOH) softwood
290 bleached kraft pulps.

291 Similarly, dissolving pulp and the CNCs produced from it using 64% H_2SO_4 were
292 analyzed using Raman spectroscopy (Fig. 8). Both these materials were found to contain
293 cellulose II (Table 2), although their concentration of cellulose II varied significantly. Compared
294 to the CNCs, the dissolving pulp contained ~ 2.5 times cellulose II (Table 2). This difference
295 indicated that the acid hydrolysis was partly successful in removing cellulose II from the
296 substrate.

297

298

299

Table 2: Estimated amount of cellulose II

Sample	Cellulose II, %
10% NaOH-treated Kraft pulp	35.5
Dissolving pulp (DP)	35.2
DP CNCs	13.6
FMC Avicel C	90.0

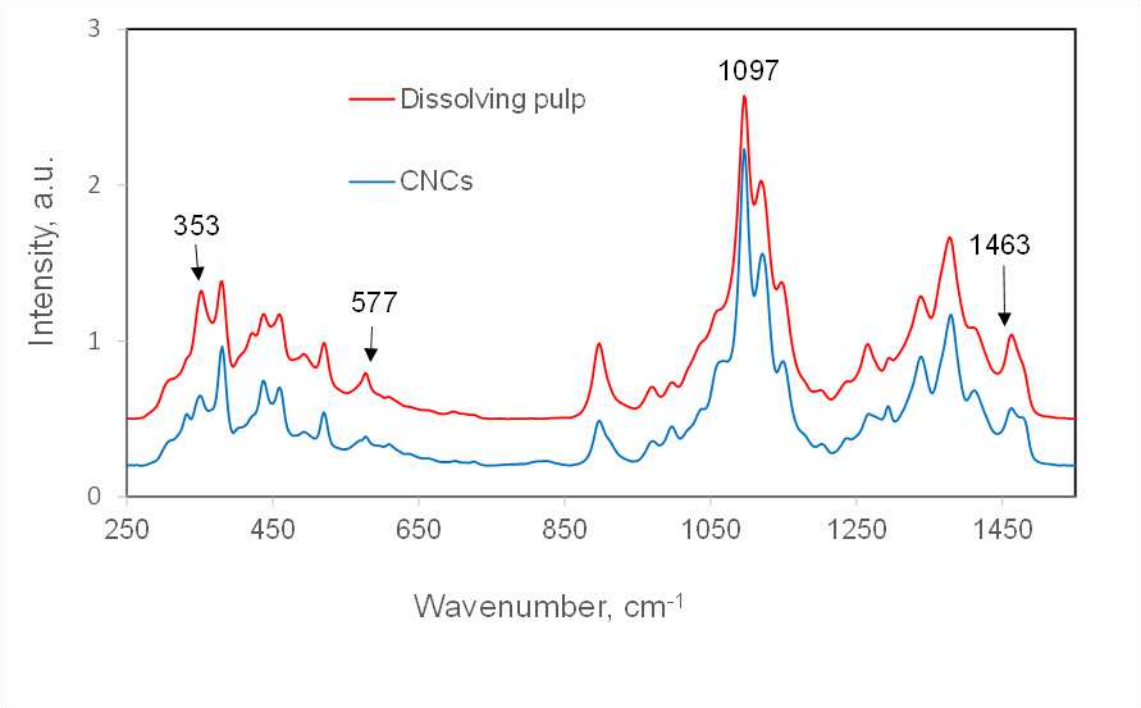

Fig. 8: Comparison of Raman spectra of dissolving pulp and CNCs.

Lastly, a commercial product, Avicel C, was analyzed and was found to consist of 90% cellulose II (Table 2). Although its spectrum is not shown here, it contained all of the spectral

features of cellulose II (Table 1) including the peaks due to the H-boned OH groups at 3445 and 3490 cm^{-1} (Šturcová et al., 2003).

In summary, the calibration method developed here appears to be a reliable method for quantifying the amount of cellulose II present in the materials. The Raman method presented in this study is more sensitive than the XRD which only detects the crystallinity of cellulose II.

CONCLUSIONS

FT Raman spectra and X-ray diffraction of cellulose II-containing materials were obtained. Compared to the XRD data, the 577 cm^{-1} Raman peak method was found to be more sensitive for detecting cellulose II. Additionally, this band was used to develop a Raman quantitation method using a set of samples that varied in their cellulose II content. When the ratios of this peak intensity to that of the 1096 cm^{-1} band I_{577}/I_{1096} were correlated with the crystalline cellulose II present in the samples, an excellent correlation was obtained ($R^2 = 0.9944$). Additionally, this Raman correlation was used to obtain the amount of cellulose II present. It is proposed that the Raman method has the potential to estimate the amount of cellulose II polymorph in various cellulose products.

Ethics Declarations

Funding: Not applicable

Conflicts of interest/Competing interests: There are no conflicts of interest to declare.

Availability of data and material: Data and materials are available

Code availability: Not applicable

Authors' contributions: All the authors contributed to this manuscript. UPA conceived and designed the study, carried out many of the Raman experiments, analyzed data and wrote the manuscript. SAR carried out numerous experiments and prepared cellulose II and amorphous cellulose; CB obtained the XRDs and performed data analysis; RSR prepared the cellulose nanocrystals from dissolving pulp.

Ethics approval: The article does not contain any experiments with human participants or animals performed by any of the authors.

REFERENCES

Agarwal UP (1999) An overview of Raman spectroscopy as applied to lignocellulosic materials. In: Argyropoulos, DS (ed.) Advances in lignocellulosics characterization, TAPPI Press, Atlanta, GA, pp 201–225.

Agarwal UP (2014) 1064 nm FT-Raman spectroscopy for investigations of plant cell walls and other biomass materials. Front Plant Sci 5, 490.

Agarwal UP (2019) Analysis of Cellulose and Lignocellulose Materials by Raman Spectroscopy: A Review of the Current Status. Molecules 24:1659–1924.

Agarwal UP, Ralph SA (1997) FT-Raman spectroscopy of wood: identifying contributions of lignin and carbohydrate polymers in the spectrum of black spruce (*Picea mariana*). Appl Spectro 51:1648–1655.

Agarwal UP, Ralph SA, Baez C, Reiner RS (2021a) Contributions of crystalline and noncrystalline cellulose can occur in the same spectral regions: Evidence based on Raman and IR and its implication for crystallinity measurements. Biomacromolecules 22:1357–1373.

Agarwal UP, Ralph SA, Reiner RS, Baez C (2016) Probing crystallinity of never-dried wood cellulose with Raman spectroscopy. Cellulose 23:223–231.

Agarwal UP, Ralph SA, Reiner RS, Baez C (2018) New cellulose crystallinity estimation method that differentiates between organized and crystalline phases. Carbohyd Polym 190:260–270.

356 Agarwal UP, Reiner RS, Ralph SA (2010) Cellulose I crystallinity determination using FT–
357 Raman spectroscopy: univariate and multivariate methods. Cellulose 17:721–733.

358 Agarwal UP, Reiner RS, Ralph SA, Catchmark J, Chi K, Foster EJ, Hunt CG, Baez C, Ibach RE,
359 Hirth KC (2021b) Characterization of the supramolecular structures of cellulose
360 nanocrystals of different origins. Cellulose 28:1369–1385.

361 Atalla RH (1976) Raman spectral studies of polymorphy in cellulose. Part I: Celluloses I and II.
362 Appl Poly Symp 28:659–669.

363 Atalla RH (1983) The structure of cellulose: quantitative analysis by Raman spectroscopy. J
364 Appl Poly Sci, Appl Poly Symp 37:295–301.

365 Atalla RH (1989) Patterns in aggregation in native celluloses: implication of recent spectroscopic
366 studies. In Kennedy JF, Phillips GO, Williams PA, eds. Cellulose. Ellis Horwood
367 Chichester.

368 Atalla RH, Gast JC, Sindorf DW, Bartuska VJ, Maciel GE (1980) Carbon-13 NMR spectra of
369 cellulose polymorphs. J Am Chem Soc 102:3249–3251.

370 Atalla RH, Vanderhart DL (1984) Native cellulose: A composite of two distinct crystalline
371 forms. Science 223:283–285.

372 Callegari A, Bolognesi S, Cecconet D, Capodaglio AG (2020) Production technologies, current
373 role, and future prospects of biofuels feedstocks: A state-of-theart review. Critical
374 Reviews in Environ Sci Techno. 50:384–436.

375 Chen C, Duan C, Li J, Liu Y, Ma X, Zheng L, Stavik J, Ni Y (2016). Cellulose (dissolving pulp)
376 manufacturing processes and properties: A mini-review. Bio Res 11:5553–5564.

377 Edwards HGM, Farwell DW, Webster D (1997) FT Raman microscopy of untreated natural
378 plant fibres. Spectrochim Acta Part A 53:2383–2392.

379 Foster EJ, Moon RJ, Agarwal UP, Bortner MJ, Bras J, Camarero-Espinosa S, Chan KJ, Clift
380 MJD, Cranston ED, Eichhorn SJ, Fox DM, Hamad WY, Heux L, Jean B, Korey M, Nieh
381 W, Ong KJ, Reid MS, Renneckar S, Roberts R, Shatkin JA, Simonsen J, Stinson-Bagby
382 K, Wanasekara N, Youngblood J (2018) Current characterization methods for cellulose
383 nanomaterials. Chem Soc Rev 47: 2609–2679.

384 Gierlinger N (2018) New insights into plant cell walls by vibrational microspectroscopy.
385 Appl Spectrosc Rev 53:517–551.

386 Haslinger S, Hietala S, Hummel M, Maunu SL, Sixta H (2019) Solid-state NMR method for the
387 quantification of cellulose and polyester in textile blends. Carbohyd Poly 207:11–16.

388 Hirota M, Tamura N, Saito T, Isogai A (2010) Water dispersion of cellulose II nanocrystals
389 prepared by TEMPO-mediated oxidation of mercerized cellulose at pH 4.8. Cellulose 17:
390 279–288.

391 Kanbayashi T, Matsunaga M, Kobayashi M (2021) Cellular-level chemical changes in Japanese
392 beech (Fagus crenata Blume) during artificial weathering. Holzforschung,
393 https://doi.org/10.1515/hf-2020-0229.

394 Kesari KK, Leppänen M, Ceccherini S, Seitsonen J, Väisänen S, Altgen M, Johansson L-S,
395 Maloney T, Ruokolainen J, Vuorinen T (2020) Chemical characterization and
396 ultrastructure study of pulp fibers. Mater. Today Chem. 17:100224.

Kumar H, Christopher LP, Recent trends and developments in dissolving pulp production and application. Cellulose 24:2347–2365.

Langan P, Nishiyama Y, Chanzy H (2001) X-ray Structure of Mercerized Cellulose II at 1 Å Resolution. Biomacromolecules 2:410–416.

Morgan JJ, Craciun MF, Eichhorn SJ (2019) Quantification of stress transfer in a model cellulose nanocrystal/graphene bilayer using Raman spectroscopy. Compos Sci Techno 177:34–40.

Nam S, French AD, Condon BD, Concha M (2016) Segal crystallinity index revisited by the simulation of X-ray diffraction patterns of cotton cellulose Iβ and cellulose II. Carbohyd Poly 135:1–9.

Nishiyama Y, Kuga S, Okano T (2000) Mechanism of mercerization revealed by X-ray diffraction. J Wood Sci 46:452–457.

Porro, F, Bédué O, Chanzy H, Heux L (2007) Solid-State 13C NMR study of Na-cellulose complexes. Biomacromolecules 8:2586–2593.

Reiner RS, Rudie AW (2013) Process scale-up of cellulose nanocrystal production to 25 kg per batch at the Forest Products Laboratory. In: Postek MT, Moon RJ, Rudie AJ, Bilodeau MA (eds) Production and applications of cellulose materials. TAPPI Press, Atlanta, pp 21–24

Schenzel K, Fischer S (2001) NIR FT Raman Spectroscopy– A rapid analytical Tool for detecting the transformation of cellulose polymorphs. Cellulose 8:49–57.

Schenzel K, Fischer S, Brendler E (2005) New method for determining the degree of cellulose I crystallinity by means of FT Raman spectroscopy. Cellulose 12:1971–1924.

418 Schenzel K, Almlöf H, Germgård U (2009) Quantitative analysis of the transformation process
419 of cellulose I → cellulose II using NIR FT Raman spectroscopy and chemometric
420 methods. Cellulose 16:407–415.

421 Segal L, Creely JJ, Martin AE, Conrad CM (1959) An empirical method for estimating the
422 degree of crystallinity of native cellulose using the x-ray diffractometer. Text Res J
423 29:786–794.

424 Sixta H, Anne Michud A, Lauri Hauru L, Shirin Asaadi S, Yibo Ma Y, Alistair W.T. King AWT,
425 Ilkka Kilpeläinen I, and Michael Hummel M (2015) - Ioncell-F: A High-strength
426 regenerated cellulose fibre. Nord Pulp Paper Res J 30:43–57.

427 Šturcová A, His I, Wess TJ, Cameron G, Jarvis MC (2003) Polarized Vibrational Spectroscopy of
428 Fiber Polymers: Hydrogen Bonding in Cellulose II. Biomacromolecules 2003, 4:1589–
429 1595.

430 Wada M, Heux L, Sugiyama J (2004) Polymorphism of cellulose I family: Reinvestigation of
431 cellulose IV_I. Biomacromolecules, 5:1385–1391.

432 Wada M, Nishiyama Y, Langan P (2006) X-ray structure of ammonia-cellulose I: New insights
433 into the conversion of cellulose I to cellulose III_I. Macromolecules, 39: 2947–2952.

434 Wiley J, Atalla RH (1987) Band assignments in the Raman spectra of celluloses. Carbohyd Res,
435 160:113–129.

436 Xing L, Gu J, Zhang W, Tu D, Hu C (2018) Cellulose I and II nanocrystals produced by sulfuric
437 acid hydrolysis of Tetra pak cellulose I. Carbohyd Poly 192: 184-192.

438 Zugenmaier P (2010) Crystalline Cellulose and Cellulose Derivatives: Characterization and
439 structures. Springer-Verlag, Berlin, Germany, Chapter 5.